WIND ENERGY
Wind Energ. 2010; **13**:279–296
Published online 9 September 2009. DOI: 10.1002/we.337

RESEARCH ARTICLE

Wind climate from the regional climate model REMO

Xiaoli Guo Larsén[1], Jakob Mann[1], Jacob Berg[1], Holger Göttel[2] and Daniela Jacob[2]

[1] Wind Energy Department, Risø National Laboratory for Sustainable Energy, Technical University of Denmark, Copenhagen, Denmark
[2] Max Planck Institute for Meteorology, Hamburg, Germany

ABSTRACT

Selected outputs from simulations with the regional climate model REMO from the Max Planck Institute, Hamburg, Germany were studied in connection with wind energy resource assessment. It was found that the mean wind characteristics based on observations from six mid-latitude stations are well described by the standard winds derived from the REMO pressure data. The mean wind parameters include the directional wind distribution, directional and omni-directional mean values and Weibull fitting parameters, spectral analysis and interannual variability of the standard winds. It was also found that, on average, the wind characteristics from REMO are in better agreement with observations than those derived from the National Centers for Environmental Prediction/National Center for Atmospheric Research (NCEP/NCAR) re-analysis pressure data. The spatial correlation of REMO surface winds in Europe is consistent with that of the NCEP/NCAR surface winds, as well as published observations over Europe at synoptic scales. Therefore, REMO outputs are well suited for wind energy assessment application in Northern Europe. Copyright © 2009 John Wiley & Sons, Ltd.

KEYWORDS
regional climate model; REMO; NCEP/NCAR re-analysis data; mean wind climate

Correspondence
X. G. Larsén, Wind Energy Department, Risø National Laboratory for Sustainable Energy, Technical University of Denmark, Copenhagen, Denmark.
E-mail: xiaoli.guo.larsen@risoe.dk

Contract/grant sponsor
Danish Research Agency; contract/grant number: 2104-04-0005.

Received 29 April 2008; Revised 26 March 2009; Accepted 30 March 2009

1. INTRODUCTION

In searching for potential locations for wind parks, very often it is found that observations are sparse or lacking, especially in remote places such as offshore where many new wind parks are expected to be built. For offshore wind resource assessment, engineers have tested other sources in addition to mast observations, e.g. satellite synthetic aperture radar (SAR) wind maps;[1] buoy and ship observations;[2] mesoscale and microscale modeling, e.g. MM5, KAMM and WAsP;[3,4] as well as general circulation models (GCMs) and regional climate models (RCMs).[2,5]

While the various methodologies have their own advantages and disadvantages, re-analysis data from GCMs, e.g. the National Centers for Environmental Prediction/National Center for Atmospheric Research (NCEP/NCAR) re-analysis data,[6] have shown to be promising for presenting temporal and spatial variation of wind climate because of their continuous assimilation of observations. However, for the purpose of finding wind park locations, the resolution of the simulated winds from GCMs is too coarse.

An RCM is nested into a large-scale forcing, which could be provided by a GCM. An RCM run at suitable resolution resolves small-scale atmospheric circulations, for instance those affected by orography or by details of the land surface;[7] moreover, it is able to simulate atmospheric processes on climatological time scales through the boundary conditions provided by GCM simulations. This physically based technique was applied in the REgional climate MOdel (REMO) from the Max Planck Institute for Meteorology in Hamburg. In recent years, RCMs, including REMO, have proven to be useful tools for analysis of regional energy and water cycles, as well as for predicting climate change at regional scale.[8–10]

In this study, to investigate whether the REMO outputs can be used for wind energy assessment, its characteristic wind parameters are derived and examined to determine whether they can provide consistent statistics with those

given by observations from Denmark, Germany and Gulf of Suez. The length of the observations varies from 3 to 24 full years, with the start year earliest 1978 and the end year latest 2005. At the same time, the wind statistics from REMO are also compared to those estimated from the NCEP/NCAR re-analysis data. The NCEP/NCAR re-analysis data in the period of 1979–2005 are used here. The start year 1979 was chosen because before 1979, the data assimilation involved a limited amount of meteorological observations, and some of these are erroneous,[11] and the end year 2005 was chosen because the full-year site observations end at 2005.

Using observations at different sites with different periods and lengths will raise the question: how representative are they for the wind climate? The World Meteorological Organization suggests a period of 30 years, and in the IPCC report 2007 (http://www.ipcc.ch/ipccreports/ar4-syr.htm), 20 years were used to illustrate the climate change. In wind energy application, 5 or more years of data are suggested to give a reasonable wind energy assessment (see e.g. Sempreviva *et al.*[12]). Here, in order to see the effect of limited data length and the effect of different periods, we will examine the interannual variability of the wind parameters derived from the observations, the REMO and NCEP/NCAR data. The wind statistics from the three different data sets are compared for their overlapping period, and these statistics are again compared to the statistics calculated for the entire period of each data set. Based on this investigation, we evaluate the simulated surface 10 m winds from REMO in the North Sea with a limited number of years of satellite data.

In the following, we will first give some details of the model REMO in 'The RCM REMO', and then briefly describe the observations and the stations in 'Measurements'. We introduce the 'standard wind' in 'Calculating the Standard Wind'. This parameter provides a possibility to compare point wind observations with the spatially averaged model values. The results of the wind parameters based on the standard winds are presented in 'Wind Parameters Based on the Standard Winds Derived from REMO Pressures, Observations and NCEP/NCAR Re-analysis Pressures'. In 'Spatial Wind Variations', the modeled mean 10 m winds from REMO are compared to satellite data in two limited areas in the North Sea, and the spatial correlation of the REMO 10 m winds is studied together with that of the NCEP/NCAR re-analysis surface winds. Discussions and conclusions follow in 'Summary and Discussion' and 'Conclusions'.

2. THE RCM REMO

The RCM REMO[8,9,13] is a three-dimensional, hydrostatic atmospheric circulation model. Like most other RCMs, REMO was developed starting from an existing numerical weather prediction model: the Europa-Modell (EM) of the German Weather Service DWD.[14] Additionally, the physical parameterization package of the GCM ECHAM4[15] has been implemented, optionally replacing the original EM physics. In numerical studies, the latter combination (i.e. the EM dynamical core plus the ECHAM4 physical parameterization scheme) proved its ability to reproduce realistically regional climatic features and is therefore used as the standard setup in recent applications, including the present study.

The lateral boundary conditions for REMO are provided by the European Center for Medium-range Weather Forecasting (ECMWF) re-analysis data (ERA-15) for the period 1979–1993, and by the operational analysis of the ECMWF for the period 1994–2003, applying a one-way nesting technique. This means that observations were not assimilated directly into REMO, only indirectly through the ECMWF data. Hereinafter, we use the term 'the ECMWF data' to refer to both the ERA-15 and the operational analysis of the ECMWF.

The ECMWF data have a resolution of T106 (~120 × 120 km). REMO was first nested in the ECMWF data with a horizontal resolution of 50 × 50 km, which covers the entire European continent. Then, the results from the first nesting were used to derive the lateral boundary conditions for the second nesting by using a double nesting strategy. The second model domain covers the region of Germany, Austria, Switzerland and a part of Denmark with a horizontal resolution of 10 × 10 km. Output from both resolutions was saved every hour.

3. MEASUREMENTS

Information about the measurements is given in Table I. Among them, Horns Rev, FINO and Sprogø are offshore sites. At Horns Rev, the given period of data is free of wake effects from the wind park. The locations of the five Danish sites and FINO are displayed in Figure 1. Abu Darag is a measurement station in the Gulf of Suez, located west to the Gulf (location in Figure 2(a)). Here, controlled by the channeling effect of the gulf, about 75% of the time winds are northerly. This site is selected to represent wind dominated by mesoscale processes.

Figure 1 shows the model grid points of REMO 10 km (small dots) and REMO 50 km (medium dots), as well as NCEP/NCAR Gaussian grid (1.875°× 1.904°, large dots). The relaxation zones of both the 10 and 50 km REMO are of thickness of eight grid boxes on each side. In this zone, the values from REMO are not independent from the driving fields, i.e. the ECMWF data for the 50 km domain, and the 50 km resolution REMO data for the 10 km domain. Therefore, for the stations located in these zones (Jylex, Horns Rev and Sprogø), the results from the 10 km REMO data will not differ from those from the 50 km REMO data. At Sprogø, which is 10-grid boxes away from the 10 km domain boundary, the data from the fifth grid box are needed to derive the wind parameters according to the method used in this study (see 'Standard Winds from the Pressure Records' for details of the method). Jylex is

Wind Energ. 2010; **13**:279–296 © 2009 John Wiley & Sons, Ltd.
DOI: 10.1002/we

Table I. Measurement sites.

Site	Location	Observation period	Data coverage (%)	Height (m)
Horns Rev	(7.875 E, 55.508 N)	1999–2002	100	62
FINO	(6.588 E, 54.014 N)	1993–2003	98.7	100
Sprogø	(10.974 E, 55.331 N)	1977–1999	97.8	70
Tystofte	(11.33 E, 55.24 N)	1982–2005	96.1	39.3
Kegnæs	(9.936 E, 54.856 N)	1991–2004	99.3	24.3
Jylex	(8.449 E, 55.942 N)	1982–2002	90.7	24
Abu Darag	(32.599 E, 29.280 N)	1991–2001	86.4	24.5

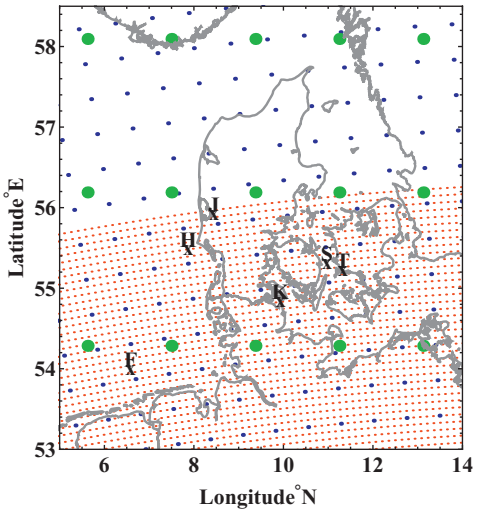

Figure 1. Grid points from different models and the locations of stations, marked by crosses and the site name initials (H stands for Horns Rev, F for FINO, S for Sprogø, T for Tystofte, K for Kegnaes, J for Jylex). The biggest bullets are the National Centers for Environmental Prediction/National Center for Atmospheric Research grid points. The medium and small dots are grid points for REMO 50 and 10 km resolution, respectively.

too close to the 10 km resolution REMO domain boundary, and there are not sufficient grid points to provide the 10 km resolution data to calculate the wind parameters. At Abu Darag, the REMO outputs are only available at the 50 km resolution.

The measured time series are 10 min averages of wind speed and direction. Missing data are found by linear interpolating between the data gap.

Information about the roughness length, roughness change and orography at Sprogø, Tystofte, Kegnæs and Jylex can be found in Kristensen *et al.*,[16] and that at Abu Darag can be found in Mortensen *et al.*[17]

4. CALCULATING THE STANDARD WIND

Maps of the modeled wind are useful in locating wind-rich areas. However, for validation, critically speaking, it is meaningless to compare the spatially averaged model winds directly with point wind measurements unless the surface conditions are homogeneous over the whole grid box. It is possible that a large part of the grid box which contains the observation site represents a very different landscape. The finer the resolution of the model, the larger the chance the surface conditions are homogeneous. However, for most of the cases, 10 km is by far not fine enough for land sites to make the direct comparison of winds possible.

4.1. Standard winds derived from the observed winds

Because of the issue mentioned earlier, most studies limit the comparison of the modeled and observed winds over water surfaces, e.g. Weisse *et al.*[18] and Winterfeldt.[19] The WAsP technique provides a possibility to extend the comparison between modeled values and point measurements to not-too-complex terrain (see Troen and Petersen;[20] www.wasp.dk). In this section, we explain how to use the WAsP technique to convert the observed wind speed to the so-called 'standard wind'. The standard wind is defined as winds at a common height, here 10 m, over a homogeneous surface with a roughness length, here 0.05 m; it is denoted by u_{st}. In 'Standard Winds from the Pressure Records', we introduce how to obtain u_{st} from model outputs of pressure. The flow diagram in Figure 3 shows the two processes through which the observed wind speed at height z, $u_{0,z}$ (the thin arrow flow) and the modeled pressures (the thick arrow flow) are used to calculate u_{st}.

When applying this technique to a nearby wind farm site, the observation has to go through the technique in two steps; see Figure 3. In step 1, we calculate the geostrophic wind at the measuring site from the surface wind by using the geostrophic drag law. First, the speedups caused by orography and roughness should be cleaned out from the wind speed at height z, $u_{0,z}$; the flat homogeneous terrain wind speed u_z can be obtained from $u_z = u_{0,z}/[(1 + s_o)(1 + s_r)]$, where s_o and s_r are speedup coefficients caused by orography and roughness change, respectively. The surface friction velocity u_*, is then determined from u_z and the area-averaged surface roughness length, z_0:

$$u_* = \frac{\kappa \cdot u_z}{\ln(z/z_0)} \quad (1)$$

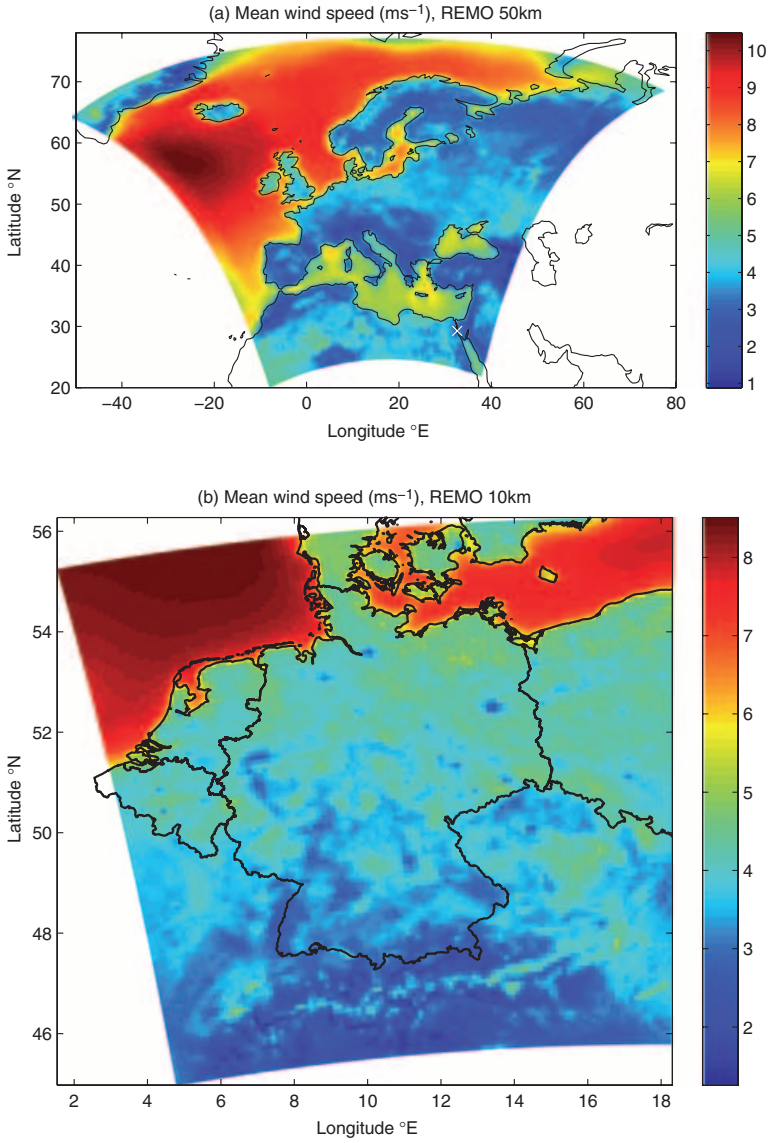

Figure 2. Twenty-five-year mean modeled wind at 10 m height over the entire domain: (a) REMO 50 km resolution; (b) REMO 10 km resolution. The location of Abu Darag (32.599°E, 29.280°N) is marked with white cross in (a).

where κ (= 0.4) is the von Kármán constant. Neutral stratification is assumed. A geostrophic wind speed G can then be calculated from u_* by using the geostrophic drag law (e.g. Tennekes[21]):

$$G = \frac{u_*}{\kappa}\sqrt{\left(\ln\frac{u_*}{f_c z_0} - A\right)^2 + B^2} \qquad (2)$$

where f_c is the Coriolis parameter, and A and B are dimensionless parameters; here, we use those of Landberg *et al.*,[22] $A = 1.8$ and $B = 4.5$.

In step 2, we assume that the geostrophic forcing over the measuring site and the turbine site are the same. Once again, we use the drag law, equation (2), now with a new roughness length of 0.05 m, to obtain a new friction velocity $u_{*,r}$ by iteration. With the new roughness length and new friction velocity, the 'standard wind' u_{st} is now obtained by using equation (1).

This technique was applied to all observations, but in a slightly different manner to the two offshore sites FINO and Horns Rev. At these two offshore sites, in the transformation of the observed wind to u_{st}, the effects of roughness change and topography over the water body are not considered (i.e. we use $u_z = u_{0,z}$). Instead, we corrected only the roughness length calculated from the Charnock formulation.[23]

When applying u_{st} to the turbine site, the programWAsP can take into account of the local effects of roughness,

Wind Energ. 2010; **13**:279–296 © 2009 John Wiley & Sons, Ltd.
DOI: 10.1002/we

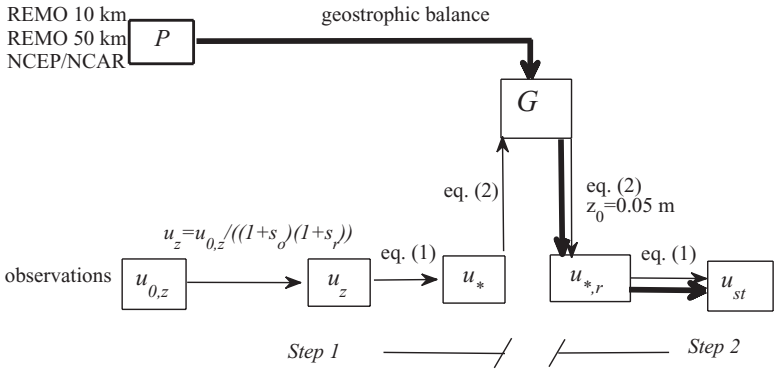

Figure 3. Flow diagram showing how the standard wind u_{st} is obtained from observed wind speed $u_{0,z}$ (thin arrow flow) and modeled pressure P (thick arrow flow). Here, s_o and s_r are speedup coefficients caused by orography and roughness change, u_z is the flat homogeneous terrain wind speed at height z, u* is the friction velocity over the area averaged surface roughness and $u^*_{,r}$ is the friction velocity over the new roughness length 0.05 m with the same geostrophic wind G.

roughness changes and orography around the site to obtain the realistic wind.

The WAsP technique is limited to not-too-complex terrain. WAsP uses the ruggedness index of a site to measure the steepness or ruggedness, and hence the complexity of the terrain around a site. According to this index, the stations used here are in the category of 'flat terrain' (the mid-latitude sites) and 'moderate complex terrain' (the Abu Darag site), so the observations can be handled by the WAsP technique. However, these limitations also restrict our validation of the REMO data to areas of such terrains.

In the transformation of the observed wind to u_{st}, the effect of stratification is not taken into account; see equations (1) and (2), and the Charnock formulation. This will introduce uncertainty to the eventual estimation of wind power potential. However, the effect of stratification is not introduced either to u_{st} through the derivation from the pressure data. The bias induced by the assumption of neutral stability should be small in the comparison to u_{st} derived from modeled pressure data and from observations.

4.2. Standard winds from the pressure records

If we treat the simulated winds from a model, either an RCM or a GCM, as the actual wind and apply the cleaning technique as described in 'Standard Winds Derived from the Observed Winds', we need appropriate input of orography, surface roughness and roughness change. This information is not directly obtainable from these models. In REMO, the corresponding roughness over a land grid box includes vegetation and orographic variances. A test of using this roughness for transformation gave completely unrealistic numbers (see Larsén and Mann[11] for more discussions on this topic). In order to avoid this problem, we derived u_{st} from the pressure field; the procedure of the derivation is indicated in Figure 3 by the thick arrow flow. This method of deriving u_{st} from the pressure data has proven to be useful in the wind engineering field.[11,24,25]

The mean sea level pressures from the grid points ($j + x$, i), ($j - x$, i), (j, $i + x$) and (j, $i - x$) were used to obtain the geostrophic wind at sea level G_{sl} at the grid point (j, i), where x is the number of grid points away from (j, i). The geostrophic balance is used, which restricts the application of this method to non-tropical regions and low terrains.

With REMO 10 km data from 2003, a sensitivity test of G_{sl} was taken with x ranging from 2 to 5 (corresponding to the pressure gradient over 40–100 km). For all grid points in the entire domain with elevation less than 300 m, on average, the mean geostrophic wind calculated with the pressure gradient over 40 and 60 km differs from that calculated with pressure gradient over 100 km by about 1.7 and 0.7%, respectively. Based on these results, we chose to calculate the pressure gradient over a distance of 100 km for both the REMO 10 and 50 km data. For the NCEP/NCAR re-analysis data, we use $x = 1$, which corresponds to wind gradient over about 400 km.

5. WIND PARAMETERS BASED ON THE STANDARD WINDS DERIVED FROM REMO PRESSURES, OBSERVATIONS AND NCEP/NCAR RE-ANALYSIS PRESSURES

In order to avoid confusion, whenever we use the term 'REMO surface winds', we mean the simulated 10 m winds from REMO, and 'NCEP/NCAR surface winds', we mean the simulated 10 m winds from the NCEP/NCAR re-analysis data.[6] By 'REMO u_{st}', we mean the standard wind u_{st} derived from the REMO pressure data. All results in this section are based on the standard wind as calculated in 'Calculating the Standard Wind'.

The statistics presented in 'Interannual Variability of the Mean Standard Wind' and 'Spectrum' are not particularly sensitive to the data length, so the entire data periods are used. This means that, for observations, the data period is as given in Table I, for REMO data, the data period is 1979–2003, and for NCEP/NCAR re-analysis data, the data period is 1979–2005. In 'Mean Standard Wind and the Weibull Fitting Parameters', we compare observed and modeled wind statistics both for the intersecting period and the entire data sets. In general, for the long observation periods we use, the differences are insignificant.

5.1. Interannual variability of the mean standard wind

It is often worthwhile to correlate short wind time series measured at a potential wind park site to longer re-analysis series. This is done to avoid being biased by unusual years present in the short time series. It is therefore of utmost importance to judge whether re-analysis models and regional models are able to account for the interannual variation of the mean wind speed.

The interannual variation of the annual mean u_{st} based on 6 h values, denoted as $\overline{u_{st,y}}$, is presented in Figure 4. The effect of using different disjunct sampling intervals on the mean values is discussed later in 'Mean Standard Wind and the Weibull Fitting Parameters'. The mean difference between the observed $\overline{u_{st,y}}$ and that of the different models was calculated for the overlapping period, and the numbers are given in Table II. The table also lists the correlation coefficients of $\overline{u_{st,y}}$ between different data sets. $\overline{u_{st,y}}$ derived from the REMO 10 km data is almost indistinguishable from those from the 50 km data.

Figure 4 shows that u_{st} derived from REMO seems to have captured the interannual rise and fall, as well as the overall trend of annual mean u_{st} as suggested by that derived from the observations for the overlapping period. Table II (third row) shows that for the six mid-latitude sites, $\overline{u_{st,y}}$ from observation and REMO are rather well correlated, although slightly less satisfying at FINO, and there is also a very good correlation between $\overline{u_{st,y}}$ from REMO and NCEP/NCAR (last row). However, at Abu Darag, while $\overline{u_{st,y}}$ from REMO can still capture the interannual variability, the strength of the wind is underestimated; see Figure 4. On the other hand, $\overline{u_{st,y}}$ from NCEP/NCAR data totally missed the interannual variability (with correlation coefficient = 0.29) and the wind strength.

For most sites, the mean difference in $\overline{u_{st,y}}$ is smaller between REMO and observations than that between NCEP/NCAR and observations, but the interannual variations are captured slightly better by NCEP/NCAR.

5.2. Spectrum

The temporal variations of the wind are important for the ability to forecast the energy production from a wind turbine park. The spectrum is a statistical measure of these variations. The power spectra of the wind time series for each of the sites and the closest grid point were calculated from the time series of u_{st} using fast Fourier transform. The averaging time for the observations is 10 min. The REMO data are saved each hour, and the NCEP/NCAR data every 6 h. The presentation of the spectrum is not sensitive to the data length, although short time series normally brings larger scatter, especially in the low frequency ranges, for which the short data set from Horns Rev is an example.

Figure 5 shows that at the mid-latitude sites, both the spectra from REMO and the NCEP/NCAR data capture the energy containing range as suggested by the spectrum from observations. The peak showing the seasonal variation of u_{st}, at 1 year^{-1}, i.e. $f = 0.0027$ day^{-1}, is well captured by both the REMO and NCEP/NCAR u_{st}. However, the diurnal wind speed variation at $f = 1$ day^{-1} at the three land sites from Denmark is absent in the spectra derived from the REMO and NCEP/NCAR u_{st}. The variations of u_{st} at scales smaller than half day are of course absent in the NCEP/NCAR data, and quite surprisingly, vanishingly small in both REMO 10 and 50 km data. At Abu Darag, the REMO spectrum describes well the wind variation, while the NCEP/NCAR spectrum significantly underestimates the level of the wind variation as suggested by the observed spectrum, clearly showing the favorable effect of the higher resolution of REMO.

5.3. Mean standard wind and the weibull fitting parameters

The following mean wind parameters are examined: the omni-directional mean standard wind speed $\overline{u_{st}}$ and its standard deviation $\sigma_{u_{st}}$, Weibull fitting scale parameter A_w and shape parameter k. In addition, for each site, the sector-wise distribution of frequency, mean u_{st} and theWeibull fitting shape parameter k are plotted in Figure 6. The sector-wise scale parameter is very similar to the sector-wise mean u_{st} and is therefore not plotted. Data are divided into 12 sectors 1, 2, 3, . . . , 12, corresponding to direction intervals 345–15°, 15–45°, 45–75°, . . . , 315–345°.

Because of the time resolution of the NCEP/NCAR data, we used 6 h values for all. Thus, there is a risk that the effect of the local diurnal variation may be missed, and also the information with $f > 2$ day^{-1} in the spectra was in fact neglected. Accordingly, the numbers shown in Table III, as well as in Figure 6, do not contain information of winds with scales smaller than 6 h. The ratios of the mean u_{st} at different time stepping ranging from 10 min to 6 h were calculated for observations and the REMO data. The difference caused by different time stepping turns out to be very small; it is on average less than 1% and it reaches 2% in the observations at Abu Darag where the half-day variation is strong (see the spectrum in Figure 5).

The statistics has been calculated with u_{st} from observations, REMO and NCEP/NCAR data for each of their entire period and their overlapping period. The results are presented in Table III and Figure 6.

Wind Energ. 2010; **13**:279–296 © 2009 John Wiley & Sons, Ltd.
DOI: 10.1002/we

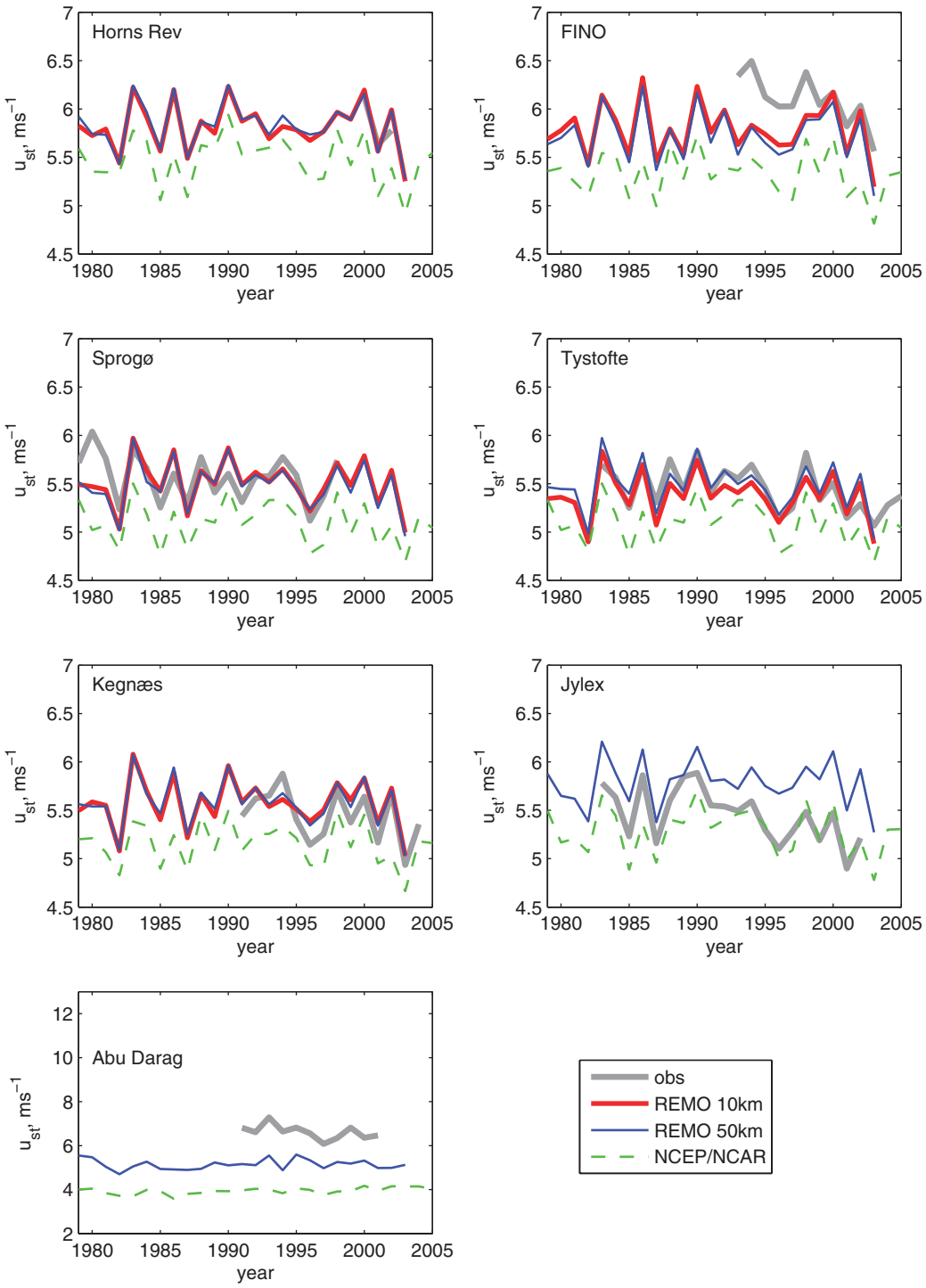

Figure 4. Time series of the annual mean u_{st} at the seven sites.

Table II. Mean annual wind bias (first two rows) and correlation coefficient (the following three rows) among different data.

Site	HO	FI	SP	TY	KE	JY	AB
$\overline{u_{st,y,OBS} - u_{st,y,REM50km}}$ (ms^{-1})	00–03	93–03	79–98	82–03	91–03	83–02	91–01
	–0.05	0.41	0.01	–0.04	–0.09	–0.38	1.39
$\overline{u_{st,y,OBS} - u_{st,y,NCEP/NCAR}}$ (ms^{-1})	00–03	93–03	79–98	82–05	91–04	83–02	91–01
	0.42	0.79	0.41	0.35	0.31	0.13	2.64
Correlation coefficient$_{OBS,REMO50km}$	00–03	93–03	79–98	82–03	91–03	83–02	91–01
	0.89	0.64	0.73	0.85	0.90	0.76	0.54
Correlation coefficient$_{OBS,NCEP/NCAR}$	00–03	93–03	79–98	82–05	91–04	83–02	91–01
	0.99	0.82	0.83	0.88	0.84	0.78	0.29
Correlation coefficient$_{REMO50km,NCEP/NCAR}$	79–03	79–03	79–03	79–03	79–03	79–03	79–03
	0.85	0.81	0.87	0.86	0.86	0.86	0.58

The overlapping data period for each calculation at each site is indicated above the results, where '79–03' means from 1979 to 2003. The sites are indicated by the first two letters of their names: Horns Rev, FINO, Sprogø, Tystofte, Kegnaes, Jylex and Abu Darag.

In Table III, the mean difference of all sites in $\overline{u_{st}}$ between the overlapping period and the entire period is negligible for observations, being 0.7% for REMO 10 km data, 0.8% for REMO 50 km data and 0.5% for NCEP/NCAR data, and the maximum difference is 1.7% for REMO 10 km data, 1.4% for REMO 50 km data and 0.9% for NCEP/NCAR data. The statistics shown in Figure 6 are for the entire period of each data set; it is similar for the overlapping period. Instead of using the NCEP/NCAR data from 1979 to 2005, truncating the data to the same period as the REMO data, i.e. 1979–2003, gives a difference in $\overline{u_{st}}$ 0.001 ms^{-1} or less at the six mid-latitude sites, and 0.01 ms^{-1} at Abu Darag. In short, the statistics in the overlapping period are almost the same as that in the entire period. This is a clear indication that the different data length and period as given by the observations here will not give bias in wind energy estimation for these sites, and such data length and period are able to represent a reasonable wind climate in this region.

Table III also suggests a general good agreement between wind parameters derived from observations and from the REMO data. At Abu Darag, REMO performs better than the NCEP/NCAR data, but still underestimates u_{st} by ~17%. The width of the Gulf of Suez is about 50 km, and only less than 10 grid points cover the entire Gulf. The 50 km resolution of REMO in this region is not enough to resolve entirely the channeling effect. The REMO-derived u_{st} deviates from the observation-derived u_{st} by up to 8% at other sites.

Figure 6 suggests that, for the six mid-latitude sites, wind parameters derived from the REMO and NCEP/NCAR pressure data capture well the sector-wise data distribution, with the prevailing winds from sectors 8–11 and a second peak of wind occurrence in sectors 4 and 5. All curves suggest that the winds are strongest in the prevailing wind sectors. The Weibull fitting shape parameter k derived from the REMO data in some cases showed rather considerable difference from the observations, a difference which was absent in the omni-directional cases. The cause were the small samples used in some of the sectors.[26]

The plots for Abu Darag (last row of Figure 6) show that in the prevailing wind sectors (sectors 1 and 12), u_{st} derived from the observations is larger than that from the REMO data, which again is larger than that from the NCEP/NCAR data.

In brief, the difference in the mean wind parameters based on u_{st} from the two REMO outputs, 10 and 50 km, is small, and for the mid-latitude sites, REMO gives better estimation of the mean u_{st} than the NCEP/NCAR data. At Abu Darag, the magnitude of u_{st} is underestimated by the REMO 50 km data and by NCEP/NCAR data.

6. SPATIAL WIND VARIATIONS

In contrast to 'Wind Parameters Based on the Standard Winds Derived from REMO Pressures, Observations and NCEP/NCAR Re-analysis Pressures', which was based on the standard wind, the analysis in this section was based on model simulations of the 10 m wind speeds and satellite data of the 10 m wind speed which is also a spatial average.

6.1. Mean surface wind distribution of REMO

The simulated 10 m wind speeds from REMO are averaged over the period 1979–2003, and are presented in Figure 2(a) (50 km resolution) and (b) (10 km resolution), respectively, for the full model domains. In Figure 2(a), the eight outmost points toward all four boundaries are in the relaxation zone; they should be disregarded when analyzing the data. The contour lines of the mean values of the simulated wind speeds for the North Sea offshore area are displayed in Figure 7(a).

There is consistency between Figure 7(a) and the mean wind map derived from ERS-2 SAR images in Hasager *et al.*[1] (their figure 6(b)) where the 10 m wind above sea level was presented for the water region 55.2–55.8 N and 7.5–8.3 E. In quantifying offshore wind resources with

Wind Energ. 2010; **13**:279–296 © 2009 John Wiley & Sons, Ltd.
DOI: 10.1002/we

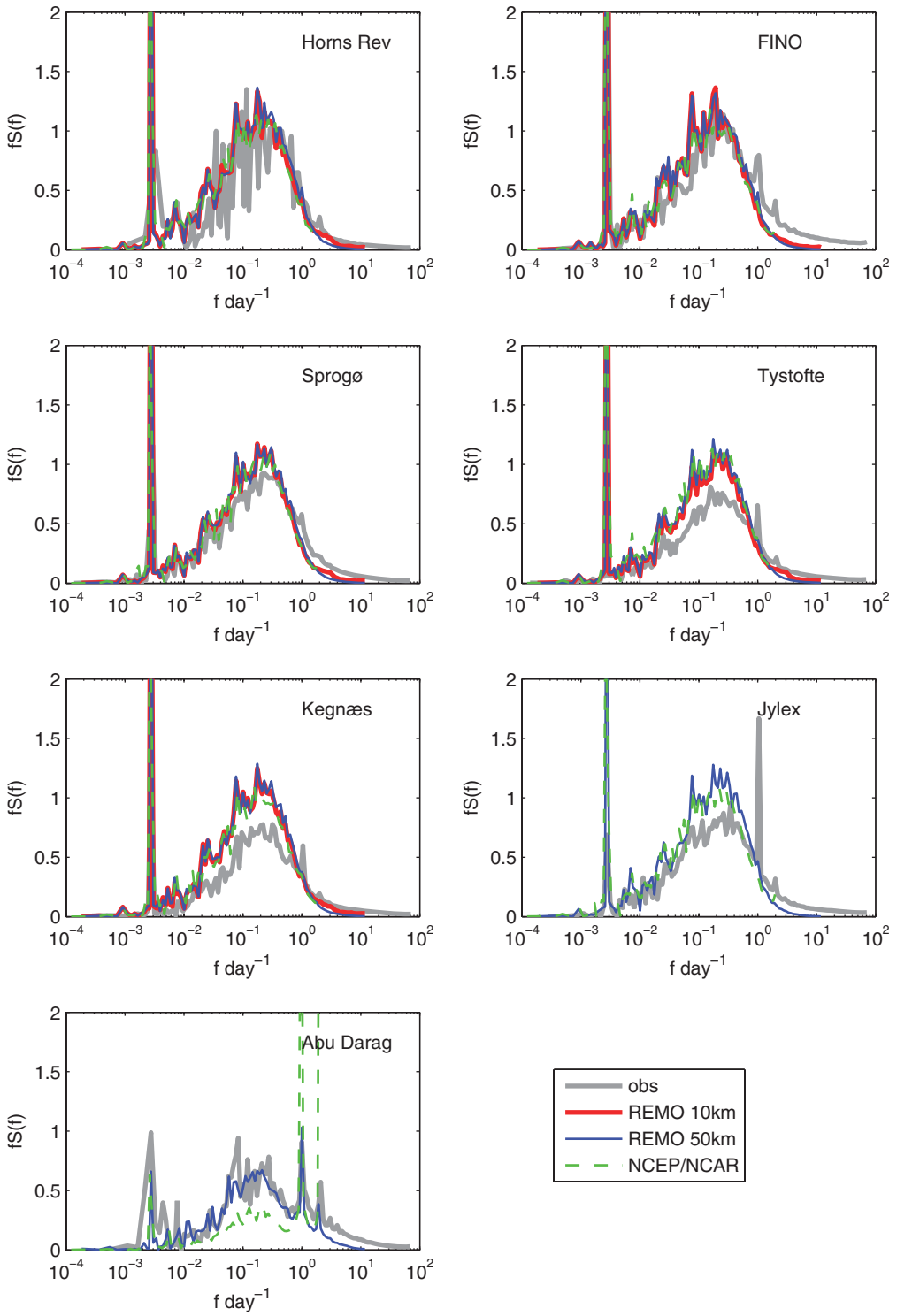

Figure 5. Spectra of the time series of u_{st} at the seven sites. For the spectra from the observations, the entire observational period is used, for those from the REMO u_{st} data are from 1979 to 2003 and for those from the National Centers for Environmental Prediction/National Center for Atmospheric Research data are from 1979 to 2005.

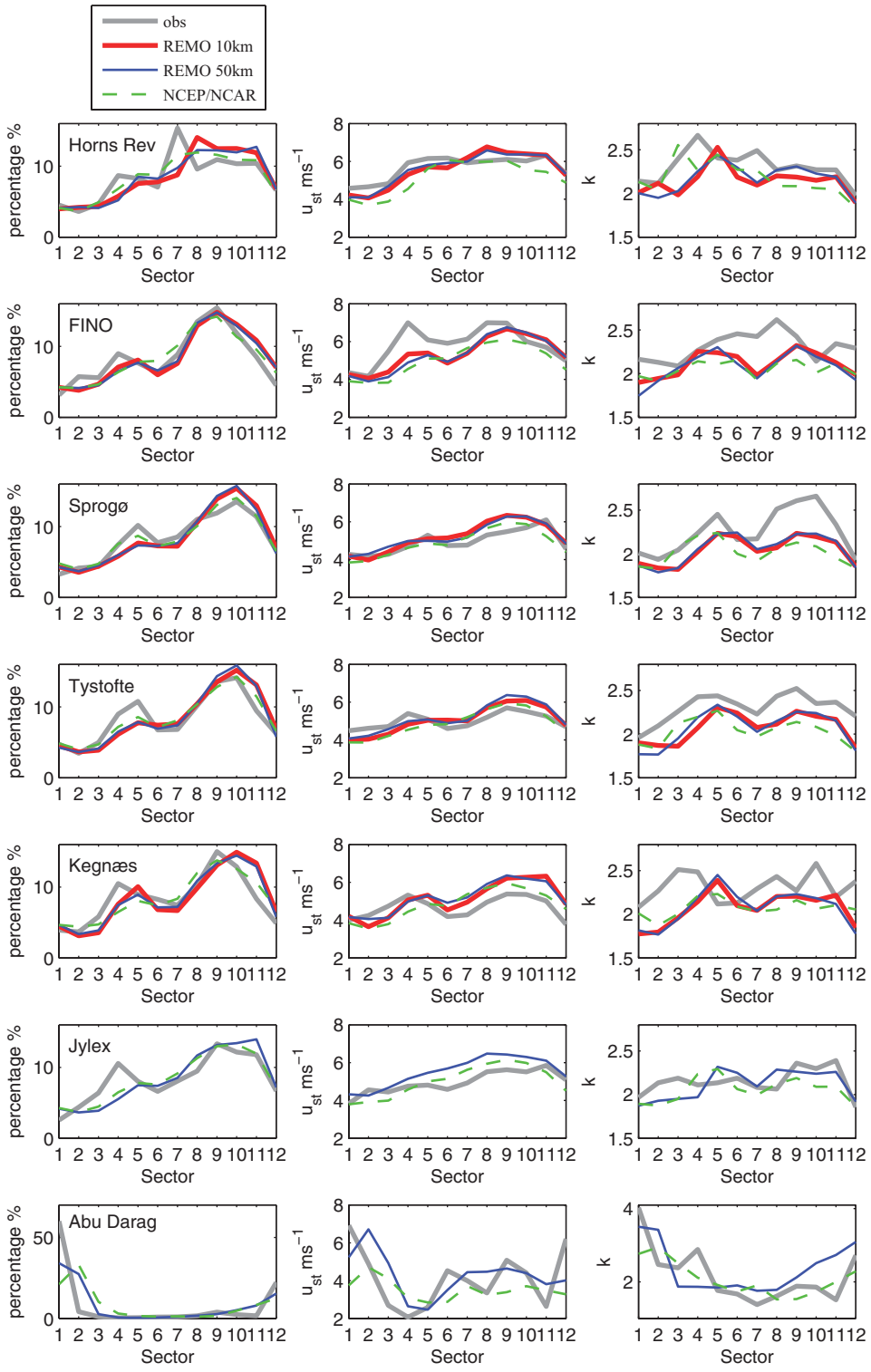

Figure 6. Directional distribution of data (left), $\overline{u}_{st}$ (middle), Weibull fitting shape parameter k (right) at seven stations, each row for one station. The information of the data periods is the same as Figure 5.

Wind Energ. 2010; **13**:279–296 © 2009 John Wiley & Sons, Ltd.
DOI: 10.1002/we

Table III. Omni-directional mean wind parameters at the seven sites.

Site	Data	Overlapping period				Entire period			
		$\overline{u_{st}}$	$\sigma_{u_{st}}$	A_w	k	$\overline{u_{st}}$	$\sigma_{u_{st}}$	A_w	k
Horns Rev									
	Observations	5.85	2.72	6.59	2.28	5.85	2.72	6.59	2.28
	REMO 10 km	5.92	3.01	6.58	2.06	5.82	2.98	6.51	2.05
	REMO 50 km	5.90	2.93	6.54	2.12	5.83	2.92	6.53	2.10
	NCEP/NCAR	5.42	2.78	5.93	2.04	5.47	2.84	6.08	2.02
FINO									
	Observations	6.13	2.92	6.89	2.22	6.13	2.92	6.89	2.22
	REMO 10 km	5.75	2.95	6.45	2.04	5.79	2.96	6.47	2.05
	REMO 50 km	5.68	2.96	6.36	2.00	5.73	2.98	6.39	2.01
	NCEP/NCAR	5.30	2.81	5.91	1.98	5.33	2.82	5.95	1.96
Sprogø									
	Observations	5.58	2.66	6.40	2.22	5.58	2.66	6.40	2.22
	REMO 10 km	5.53	2.87	6.17	2.02	5.51	2.86	6.15	2.02
	REMO 50 km	5.51	2.83	6.16	2.04	5.48	2.82	6.14	2.04
	NCEP/NCAR	5.13	2.73	5.75	1.96	5.10	2.71	5.71	1.96
Tystofte									
	Observations	5.48	2.55	6.12	2.27	5.47	2.55	6.11	2.27
	REMO 10 km	5.41	2.79	6.04	2.03	5.38	2.78	5.99	2.02
	REMO 50 km	5.50	2.82	6.17	2.05	5.48	2.81	6.12	2.04
	NCEP/NCAR	5.11	2.71	5.72	1.96	5.10	2.71	5.71	1.96
Kegnæs									
	Observations	5.46	2.75	6.06	2.09	5.45	2.75	6.06	2.10
	REMO 10 km	5.56	2.88	6.25	2.02	5.57	2.87	6.24	2.03
	REMO 50 km	5.55	2.85	6.23	2.04	5.58	2.85	6.24	2.05
	NCEP/NCAR	5.13	2.71	5.71	1.98	5.15	2.73	5.73	1.97
Jylex									
	Observations	5.45	2.79	6.07	2.04	5.45	2.79	6.07	2.04
	REMO 50 km	5.82	2.91	6.54	2.10	5.78	2.89	6.48	2.10
	NCEP/NCAR	5.32	2.80	5.95	1.98	5.29	2.78	5.90	1.99
Abu Darag									
	Observations	6.52	2.55	7.75	2.11	6.52	2.55	7.75	2.11
	REMO 50 km	5.21	2.15	5.76	2.60	5.14	2.13	5.68	2.60
	NCEP/NCAR	3.96	1.80	4.43	2.33	3.94	1.82	4.39	2.30

The unit for the mean u_{st} ($\overline{u_{st}}$), the standard deviation of u_{st} ($\sigma_{u_{st}}$) and the Weibull fitting scale parameter A_w is ms^{-1}; k is the Weibull fitting shape parameter. Here, the numbers are obtained with the different data from the overlapping period (varying by site as shown in Table II), as well as for the entire record length, which, for the observation, can be found in Table I, for REMO data is 1979–2003 and for the NCEP/NCAR data is 1979–2005.

satellite maps in the North Sea, Hasager *et al.*[27] used 85 SAR images in the period 1999 to 2003 to visualize the mean wind variation from coastline to offshore (their figure 2); two transects, south and north to the wind farm Horns Rev, were selected and they were drawn in Figure 7(a) as thick gray lines. The average wind of the two transects from the 85 SAR images shows an increase from about 5 m s^{-1} at the coastline to 7 m s^{-1} at about 40 km offshore. Hasager *et al.*[27] recommended recent calculations with the ENVISAT data from the period 2003 to 2007 (not published), which give wind speed of about 6.5 m s^{-1} at the coastline to 8 m s^{-1} at about 40 km offshore, with the number of samples varying from about 200 close to the coast to 120 out in the ocean. The new horizontal wind profiles for the two transects from these maps were reproduced in Figure 7(b). There is a difference in the mean wind magnitude of about 1 m s^{-1} between the wind from Hasager *et al.*[27] and Figure 7(b), although the horizontal wind gradient is similar. The difference is believed to be induced by difference in sampling. Barthelmie and Pryor[28] found that for an uncertainty of ±10% at a confidence level of 90%, 50–70 randomly selected perfectly accurate images are required to characterize the mean wind speed and the Weibull fitting scale parameter A_w. But in order to obtain the Weibull fitting shape parameter k with the same certainty, Pryor *et al.*[26] suggested that approximately 250 samples are needed. Here, we examine only the mean wind speed, so the samples (assuming perfect accuracy) are sufficient to give an uncertainty within 10%.

The bullets in Figure 7(b) are the simulated 10 m winds from REMO at 10 km resolution, averaged over 1979–2003, from a row of the grid points that lies approximately between the two transects, marked with white crosses in Figure 7(a). The REMO winds and the satellite winds

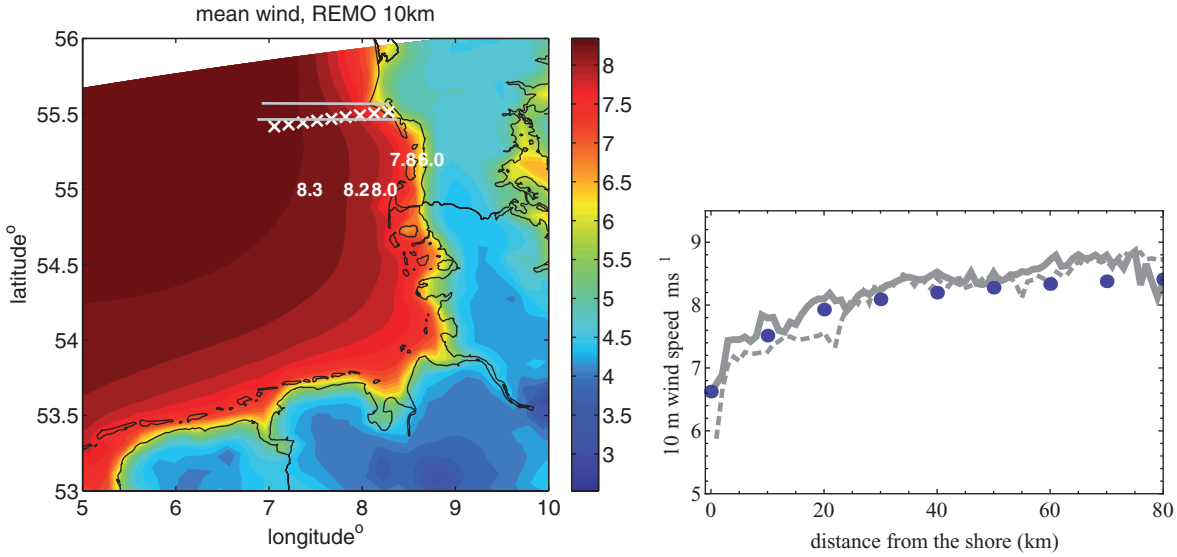

Figure 7. (a) Left, contour lines of the 25 year mean modeled wind at 10 m height from REMO 10 km data. Crosses are the transect selected for study of wind profile simulated from REMO offshore. The two gray solid lines are the two transects from Hasager *et al.*,[27] where the satellite data are available. (b) Right, variation of wind speeds at 10 m height with distance from the shore. Bullets: REMO 10 km winds from the grid points marked with white crosses in (a). Curves: ENVISAT winds from 2003 to 2007 for the two transects: solid for the northern and dashed for the southern.

agree very well. Although the wind speeds are still increasing 20 km from the coast in this area, the increase is very small, suggesting that in terms of maximizing wind resources at this location, it is not necessary to go beyond this distance.

Unfortunately, the overlapping period of the REMO data and the satellite data is too short: only 2003. This means there are too few satellite images to make meaningful averages. In making the comparison, we have assumed that both the REMO surface winds (1979–2003) and the satellite winds (2003–2007) are representative of the mean wind climate. Based on the interannual variability of the mean standard winds throughout 1978–2005 as presented in 'Interannual Variability of the Mean Standard Wind', this assumption could be considered reasonable, and it suggests that using 5 years of data (the length of the satellite data) will not give significant deviation from the 25 year mean.

In addition to the sample size, the satellite-derived winds suffer from uncertainties because of spatial resolution of the images and the techniques, etc. The uncertainties in relation to the sample size are usually not evenly distributed over a larger area, and that is the reason we cannot make such a comparison of the satellite-derived winds with the REMO simulated winds over the entire North Sea, but restrict it to quite limited areas where the wind climate has already been well studied.

In this section, the satellite-derived winds are only compared to the REMO simulated 10 m winds because such a fine resolution variation of wind speed could not be seen in the NCEP/NCAR re-analysis data of about 200 km resolution, nor is it expected in the ECMWF data of 120 km resolution. Such a spatial variation of the surface wind speed simulated from the REMO is clearly an added value to the ECMWF data.

6.2. Spatial correlation of the surface winds

Spatial correlations of winds at large scales are important for the estimation of wind power fluctuations from wind parks scattered over a region.[29,30] In this section, the spatial correlation is examined for the simulated 10 m winds from REMO. It is compared to that of the NCEP/NCAR re-analysis 10 m winds. We examine the spatial correlation of the surface winds in different climatological zones. It will be demonstrated that the spatial correlation is dependent on the surface conditions, by studying areas with only water surface and areas with land–water mixed surface within the different zones. The averaging time is another factor that affects the wind correlation in space. Therefore, the correlation parameters are estimated from time series of the surface winds with the averaging time ranging from 1 year to the original time resolution of the data (i.e. it is 1 h for the REMO surface winds, and it is 6 h for the NCEP/NCAR re-analysis surface winds).

Three different regions are depicted in Figure 8: Northern Europe (zone A); Southern Europe (zone B); and an area covering most of Europe, 35–68°N and 17°W–35°E (zone C). The correlation parameters for every pair of grid points inside each zone are calculated. The following is the list of zones and corresponding grid points from REMO and the NCEP/NCAR model.

Wind Energ. 2010; **13**:279–296 © 2009 John Wiley & Sons, Ltd.
DOI: 10.1002/we

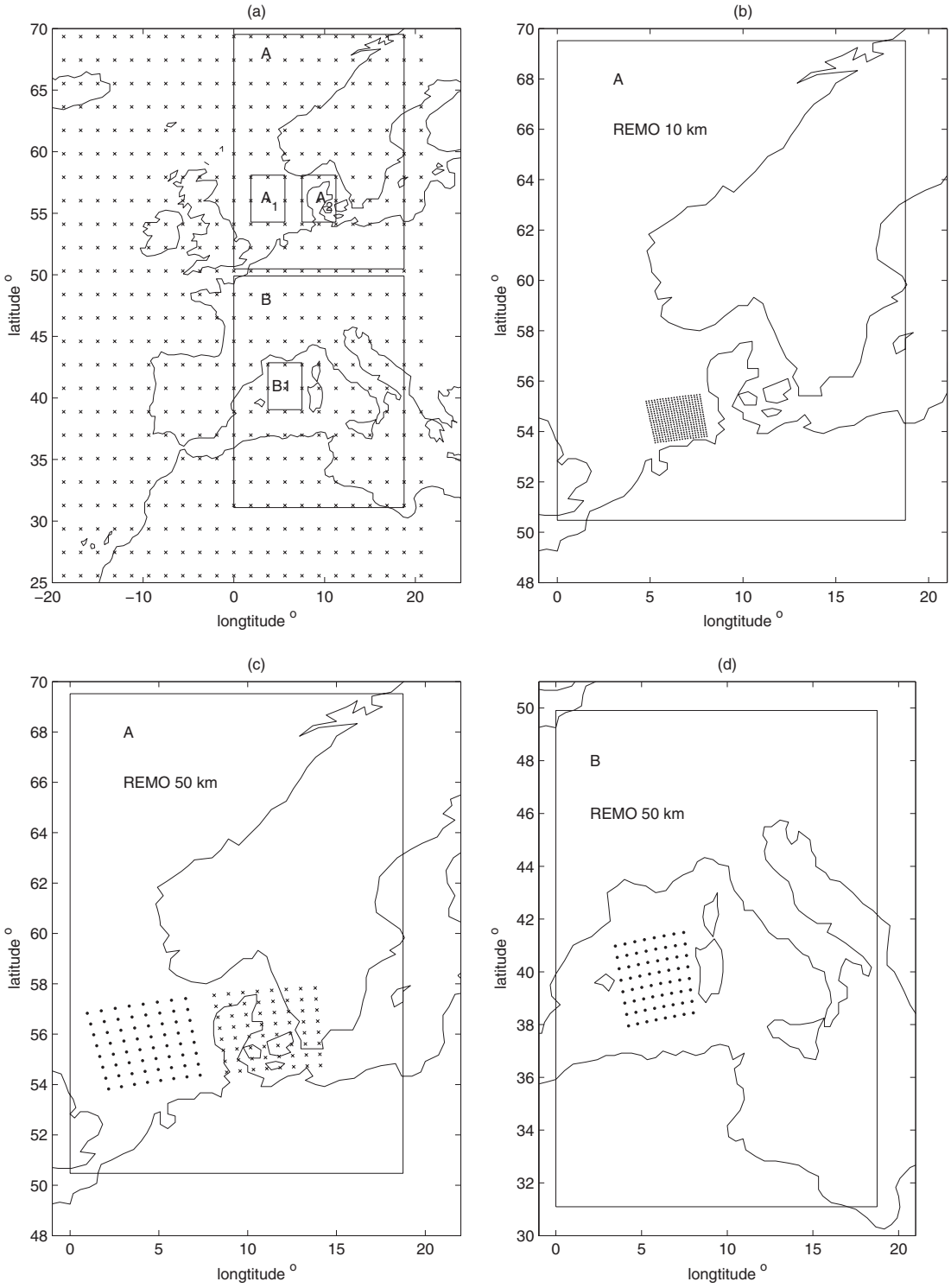

Figure 8. (a) Zones A and B, the grid points from National Centers for Environmental Prediction/National Center for Atmospheric Research (NCEP/NCAR) are marked. A_1 and A_2 are two subzones in zone A representing water and mixed surface, and B_1 is subzone with water surface in zone B, each containing 9 NCEP/NCAR grid points. (b) Within zone A, REMO 10 km data over water, 20 by 20 grid points. (c) Within zone A, two areas of REMO 50 km resolution data, over water (•) and land (×), 8 by 8 grid points each. (d) Within zone B, REMO 50 km resolution over water, 8 by 8 grid points.

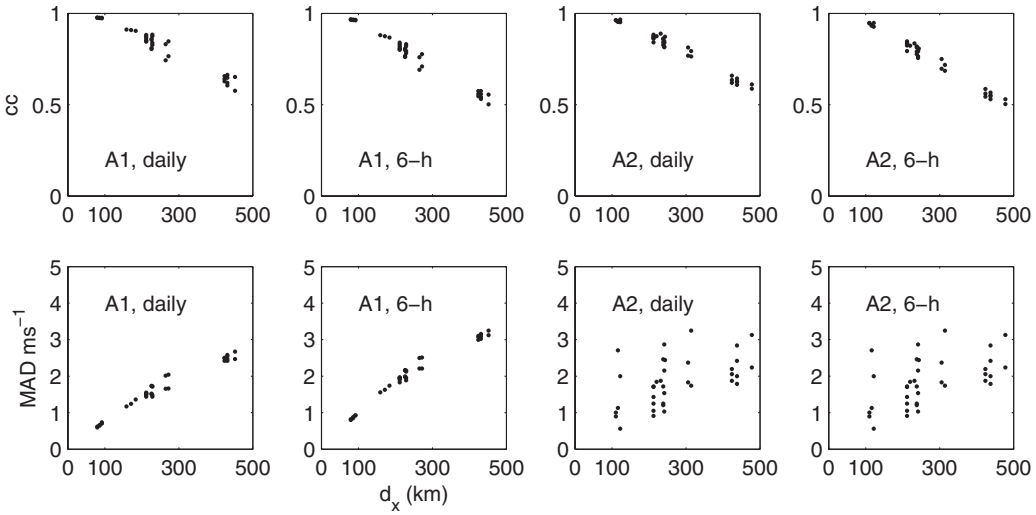

Figure 9. Spatial correlation parameters cc and MAD for zone A_1 (water) and zone A_2 (mixed water–land), see A_1 and A_2 in Figure 8(a), based on the National Centers for Environmental Prediction/National Center for Atmospheric Research surface winds with averaging time of 1 day and 6 h.

- In zone A, A_1 and A_2 from NCEP/NCAR grid points in zone A (Figure 8(a));
- In zone A, 20 by 20 water grid points from REMO 10 km, starting from the model domain boundary in the north to the coastline in the south (Figure 8(b));
- In zone A, 8 by 8 water as well as mixed land–water grid points from REMO 50 km (see Figure 8(c)); and
- In zone B, subzone B_1, containing 9 NCEP/NCAR grid points in Figure 8(a), and 8 by 8 water grid points from REMO 50 km in Figure 8(d).

Two correlation parameters are used. Normally, the correlation coefficient, here denoted as *cc*, is used to describe the spatial correlation (e.g. Pope[31]):

$$cc(i,j)=\frac{1}{n_t}\cdot\sum_{m=1}^{n_t}\frac{\left(u_{im}-\overline{u_{im}}\right)\left(u_{jm}-\overline{u_{jm}}\right)}{\sqrt{\frac{1}{n_t}\sum_i\left(u_{im}-\overline{u_{im}}\right)^2}\sqrt{\frac{1}{n_t}\sum_j\left(u_{jm}-\overline{u_{jm}}\right)^2}}$$
$$i=1,N-1;\ j=i+1,N \qquad (3)$$

where n_t is the length of the time series; u_{im} and u_{jm} are wind speed u at locations i and j, respectively, at time m; and N is the total number of locations in the area of interest. For the hourly time series from REMO, $n_t = 219{,}144$, and for the 6 h time series of the NCEP/NCAR re-analysis winds, $n_t = 39{,}448$.

The mean absolute difference (*MAD*) is another parameter to describe the correlation between two time series (e.g. Robeson and Shein[32]):

$$MAD=\frac{1}{n_t}\cdot\sum_{m=1}^{n_t}|u_{im}-u_{jm}|,\quad i=1,N-1;\ j=i+1,N \qquad (4)$$

The slow temporal variation in the time series at two sites tends to dominate over smaller-scale variations (Robeson and Shein[32]). *MAD* offsets the well-correlated slow variation in the two time series, and therefore, is expected to present better the local variations.

The difference between the *cc* and *MAD* can clearly be seen in Figure 9. The figure shows *cc* and *MAD* for every pair of grid points in zone A_1 (water) and A_2 (mixed water–land), calculated as a function of distance d_x, based on daily average and 6 h NCEP/NCAR re-analysis surface winds. Over water (A_1), both *cc* and *MAD* show a clear dependence on d_x. Over the mixed surface (A_2), *cc* with the same d_x contains very little scatter, indicating a uniform dependence of *cc* on d_x regardless of the surface roughness. At the same time, *MAD* increases with d_x with large scatter, reflecting the local scale effects. Moreover, Figure 9 suggests that using 1 day as the averaging time gives higher *cc* and smaller *MAD* than 6 h. This is a consequence that normally using longer averaging time gives smaller standard deviations.

This is also true with the REMO 50 km 10 m winds. It was found that the values of *cc* and *MAD* are no longer sensitive to the averaging time when this is reduced to about 6 h, which characterizes the local weather time scale.

Figure 10(a),(b) shows the spatial correlation of the REMO surface winds, at 10 km as well as 50 km resolutions, together with that of the NCEP/NCAR surface winds. The dependence of both *cc* and *MAD* on the distance d_x agrees well between the REMO and the NCEP/NCAR winds. This suggests that for zone A_1 in the North Sea, REMO and the NCEP/NCAR model give consistent variability in both the synoptic (in terms of *cc*) and local (in terms of *MAD*) wind systems.

Wind Energ. 2010; **13**:279–296 © 2009 John Wiley & Sons, Ltd.
DOI: 10.1002/we

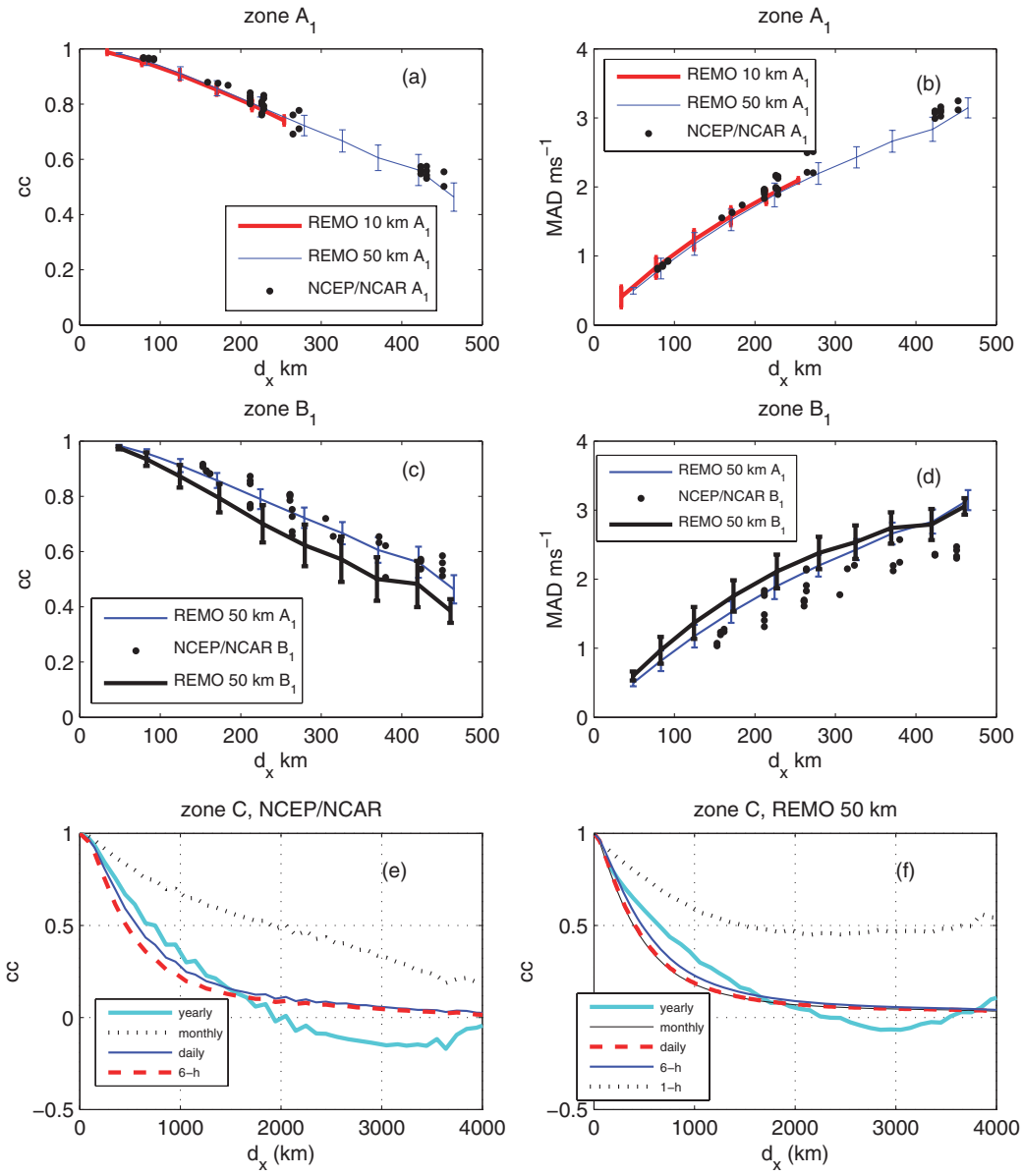

Figure 10. Spatial correlation parameters cc and MAD for A_1 (a and b), and for B_1 (c and d), based on 6 h averaging 10 m height winds. For the REMO surface winds, mean values of cc and MAD in different bins of distance d_x were plotted together with one standard deviation. (e) and (f): cc varying with distance d_x, for zone C, from National Centers for Environmental Prediction/National Center for Atmospheric Research (e) and REMO 50 km (f) surface winds.

However, in the west Mediterranean Sea zone B_1, the surface winds correlation in the NCEP/NCAR model shows slightly larger than in REMO, as suggested by both *cc* and *MAD* (Figure 10(c),(d)). This is possibly a result of the difference of the wind field between the NCEP/NCAR data and the forcing to REMO (i.e. the ECMWF data). Seemingly, the simulated winds from REMO are better correlated in the North Sea area than in the west Mediterranean Sea.

In Figure 10(e),(f), the large-scale wind variability across Europe is examined with both the REMO and NCEP/NCAR surface winds. A different averaging time is used ranging from 1 year to 1 h (or 6 h for the NCEP/NCAR winds). It seems that in this area, the average wind patterns are best correlated at the monthly time scale. For averaging time shorter than 1 day, the variation of *cc* with d_x is almost identical for the REMO and NCEP/NCAR surface winds, and the corresponding curves in Figure 10(e),(f) are in perfect agreement with that from measurements collected over Europe, given as figure 28 in Gielbel.[29] The annually averaged winds become negatively correlated at distances larger than about 2000 km, which is the

typical weather pattern scale over Europe. The scale of the Icelandic-low and Azores-high phenomenon contributes to this. The signal of the negative correlation is slightly stronger in the NCEP/NCAR surface winds. Note, if the correlation is calculated over the entire domain of REMO 50 km (see Figure 2(a)), the mean negative *cc* at distance 2000–4000 km weakens in NCEP/NCAR data and disappears in REMO data. The mean *cc* depends on the selected area where it reflects a combined effect of the scales of the different weather systems within it.

7. SUMMARY AND DISCUSSION

Characteristic parameters that are closely connected to wind energy resource assessment are derived from the output of the RCM REMO.

First, the wind statistics based on the standard wind u_{st} that are derived from the REMO data, observations and NCEP/NCAR re-analysis data are compared. The standard wind is introduced here, not only because it is directly relevant to wind energy application for a particular wind farm in connection with the WAsP method, but also because it provides a possibility to validate the spatially averaged model values with the point wind measurements in inhomogeneous terrain. Because of the limitation of the WAsP technique, the validation of the model outputs is limited to not-too-complex terrain.

When comparing models to observations, it should be remembered that there are uncertainties involved in the measuring systems. We compare directly the wind statistics obtained from 25 year REMO and NCEP/NCAR re-analysis data with observations that are normally shorter than 25 years. Thus, it has been assumed that the observations of different lengths are long enough to represent a stationary wind climate. Different data length could easily introduce bias to the mean energy prediction, but its impact on the analysis of interannual mean wind variation and the spectra is small. Both the interannual mean wind variation and the mean wind statistics clearly suggest that the different data length and period as given by the observations here will not give bias in the wind energy estimation for these sites.

We use variables that are directly relevant to wind energy applications. The characteristics of u_{st} variability, as given by the observations at the mid-latitude sites, are satisfactorily described by that derived from the REMO pressure data, including its spectrum, its omni-directional and directional mean values and its Weibull fitting parameters, as well as its interannual variability. The accurate reproduction of the spectrum up to 1 day^{-1} has encouraged engineers to consider using the outputs from REMO in modelings of wind turbine cutouts in a power system region.[33] At the same time, u_{st} derived from the NCEP/NCAR re-analysis pressure data also describes well the spectrum up to $f = 2$ day^{-1}, but the mean u_{st} is significantly underestimated in comparison to the observations. The results are less accurate at the Gulf of Suez site Abu Darag. Although its variance is well captured by the REMO, as shown by its spectrum, including the peaks at $f = 1$, 2 day^{-1}, the wind intensity is underestimated, as suggested by the mean values of the REMO u_{st}.

Second, the spatial distribution of the simulated 10 m winds from REMO has been examined. It showed consistency to earlier studies on North Sea offshore wind energy based on satellite data. Here, we only compared the REMO 10 m winds with the satellite 10 m winds in very limited areas (55.2–55.8 N, 7.5–8.3 E) and two transects across the North Sea around the offshore wind park Horns Rev. These areas have been of interest for Danish offshore wind energy assessment. In the future, such a comparison could be considered to be made over a larger area where the satellite data exist. However, when larger area of satellite data is considered, more significant uncertainties will be involved, with the unevenly distributed satellite images being one of the causes.

The spatial variation and correlation of the wind affect significantly the wind energy integrability into an electrical grid. It was found here that, for Europe, the wind variability, as described by the spatial correlation coefficient *cc* in the REMO surface wind outputs, is consistent with that in the NCEP/NCAR re-analysis surface winds, and both are in agreement with measurements provided by Gielbel.[29] We also demonstrate that the spatial correlation of the surface winds depends on the geographical area, its surface conditions, the weather patterns and the averaging time that is applied to the time series.

To emphasize, there is no direct observation assimilation to REMO; rather, the assimilation is done to REMO's driving force, namely, the ECMWF data. The wind parameters derived from REMO outputs are thus compared to two independent data sets, namely, observations and NCEP/NCAR re-analysis data in order to meet the goal of this study: to find out whether REMO can provide useful information for wind energy resource assessment. Although it is beyond the scope of this study to explore systematically the added values of REMO to its driving field, i.e. the ECMWF data, there are clearly several pieces of evidence of such added values. As to the definition of added value of wind speed, one can refer to the instantanous wind speed, or to statistical parameters derived from the wind speed time series. Here, we consider the statistical parameters. First, at Abu Darag where the width of the Gulf of Suez is about 50 km, although the 50 km resolution of REMO cannot completely resolve the channeling wind, it significantly improves the prediction of the wind strength and wind variation compared to the NCEP/NCAR re-analysis data. It cannot be expected such a channeling effect to be better resolved in the driving field of 120 km resolution. Second, the fine spatial resolution of wind distribution in the coastal areas, as shown in Figure 7, is no doubt an added value to the 120 km ECMWF data. The issue of added values from REMO has already been studied in Winterfeldt,[19] where patterns of wind speeds from REMO, ECMWF and NCEP/NCAR re-analysis data in the North Atlantic were analysed. Added values were found in the

Wind Energ. 2010; **13**:279–296 © 2009 John Wiley & Sons, Ltd.
DOI: 10.1002/we

frequency distribution in coastal areas, and in the instantaneous wind speeds for rough coastal areas with complex orography. This is consistent with our results here. We hope to systematically explore the issue of the 'added values' of REMO beyond using the ECMWF data in relation to wind energy application in a separate paper.

8. CONCLUSIONS

This study shows that:

- The wind characteristics based on u_{st} derived from the wind observations from six mid-latitude stations are well described by the REMO u_{st}.
- Wind parameters derived from REMO data are in agreement with observations, and on average, they describe the wind magnitude slightly better than the NCEP/NCAR re-analysis data.
- The modeled 10 m wind distribution from REMO is consistent with the satellite data over limited areas in the North Sea.
- The spatial correlation of REMO surface winds over Europe is consistent with that of the NCEP/NCAR surface winds in the synoptic scale, and also with published observations over Europe.

These are good indicators that the REMO outputs can be considered for wind energy assessment applications in the mid-latitudes of Europe.

ACKNOWLEDGEMENTS

This work was supported by the Danish Research Agency grant 2104-04-0005 'Offshore wind power'. We thank Dong Energy for the observations at Horns Rev, and Merete B. Christiansen and Charlotte B. Hasager for Figure 7(b); the satellite data for producing this figure are provided by the European Space Agency. We also thank Andrea Hahmann, the editor and reviewers for their valuable comments and suggestions. The NCEP/NCAR data are provided by the NOAA-CIRES Climate Diagnostics Center, Boulder, CO, from their Web site at http://www.cdc.noaa.gov/.

REFERENCES

1. Hasager CB, Nielsen M, Astrup P, Barthelmie R, Dellwik E, Jensen NO, Jørgensen BH, Pryor SC, Rathmann O. Offshore wind resource estimation from satellite SAR wind field maps. *Wind Energy* 2005; **8**: 403–419.
2. Lavagnini A, Sempreviva A, Transerici C, Accadia C, Casaioli M, Mariani S, Speranza A. Offshore wind climatology over the Mediterranean basin. *Wind Energy* 2006; **9**: 251–266.
3. Jimenez B, Durante F, Lange B, Kreutzer T, Tambke J. Offshore wind resource assessment with WAsP and MM5: comparative study for the German Bight. *Wind Energy* 2007; **10**: 121–134.
4. Badger J, Giebel G, Larsén XG, Nielsen TS, Nielsen H, Madsen H, Tøfting J. Report on the use of stability parameters and mesoscale modelling in short-term prediction. *Technical Report Risø-R-1614(EN)*, Risø National Laboratory, Roskilde, Denmark, URL:www.risoe.dk, 2007.
5. Pryor SC, Barthelmie RJ. Use of RCM simulations to assess the impact of climate change on wind energy availability. *Technical Report Risoe-R-1477(EN)*, Risø National Laboratory, Roskilde, Denmark, http://www.risoe.dk/rispubl/VEA/ris-r-1477.htm, 2004.
6. Kalnay E, Kanamitsu M, Kistler R, Collins W, Deaven D, Gandin L, Iredell M, Saha S, White G, Woollen J, Zhu Y, Celliah M, Ebisuzaki W, Higgins W, Janowiak J, Mo KC, Ropelewski C, Wang J, Leetmaa A, Reynolds R, Jenne R, Joseph D. The NCEP/NCAR 40-year reanalysis project. *Bulletin of the American Meteorological Society* 1996; **77**: 437–471.
7. McGregor JL. Regional climate modelling. *Meteorology and Atmospheric Physics* 1997; **63**: 105–117.
8. Jacob D, Bärring L, Christensen J, Christensen O, Hagemann S, Hirschi M, Kjellström E, Lenderink G, Rockel B, Schär C, Seneviratne S, Somot S, van Ulden A, van den Hurk B. An inter-comparison of regional climate models for Europe: design of experiments and model performances. *Climate Change* 2007; **81**: 31–52.
9. Jacob D, van den Hurk B, Andrae U, Elgered G, Fortelius C, Graham LP, Jackson SD, Karstens U, Käopken C, Lindau R, Podzun R, Rockel B, Rubel F, Sass BH, Smith RNB, Yang X. A comprehensive model inter-comparison study investigating the water budget during the BALTEX-PIDCAP period. *Meteorology and Atmospheric Physics* 2001; **77**: 19–43.
10. Deque M, Jones RG, Wild M, Giorgi F, Christensen JH, Hassell DC, Vidale PL, Rockel B, Jacob D, Kjellström E, de Castro M, Kucharski F, van den Hurk B. Global high resolution versus limited area model climate change projections over Europe: quantifying confidence level from PRUDENCE results. *Climate Dynamics* 2005; **25**: 653–670.
11. Larsén XG, Mann J. Extreme winds from the NCEP/NCAR reanalysis data. *Wind Energy* 2009; doi: 10.1002/we.318
12. Sempreviva AM, Barthelmie RJ, Pryor SC. Review of methodologies for offshore wind resource assessment in European seas. *Surveys in Geophysics* 2008; **29**: 471–497. doi 10.1007/s10712-008-9050-2

13. Jacob D, Podzun R. Sensitivity studies with regional climate model REMO. *Meteorology and Atmospheric Physics* 1997; **63**: 119–129.
14. Majewski D. The Europa-Modell of the Deutscher Wetterdienst. Vol. 2 of ECMWF seminar on numerical methods in atmospheric models. [Online]. Available: http://www.ecmwf.int/publications/library/ecpublications/_pdf/seminar/1991/numerical2_majewski.pdf.
15. Roeckner E, Arpe K, Bengtsson L, Christoph M, Claussen M, Dümenil L, Esch M, Giorgetta M, Schlese U, Shulzweida U. The atmospheric general circulation model ECHAM-4: model description and simulation of present-day climate. *Technical Report 218*, available from Max Planck Institute for Meteorology, Hamburg, 1989.
16. Kristensen L, Rathmann O, Hansen SO. Extreme winds in Denmark. *Journal of Wind Engineering and Industrial Aerodynamics* 2000; **87**: 147–166.
17. Mortensen NG, Hansen JC, Badger J, Jørgensen BH, Hasager CB, Youssef LG, Said US, Moussa AAE, Mahmoud MA, Yousef AES, Awad AM, Ahmed MAR, Sayed AAM, Korany MH, Tarad MAB. *Wind Atlas for Egypt, Measurements and Modelling 1991–2005*. Risø National Laboratory, New and Renewable Energy Authority and Egyptian Meteorological Authority: Cairo, 2005.
18. Weisse R, Storch HV, Feser F. Northeast Atlantic and North Sea storminess as simulated by a regional climate model during 1958–2001 and comparisons with observations. *Journal of Climate* 2005; **18**: 465–479.
19. Winterfeldt J. Comparison of measured and simulated wind speed data in the North Atlantic. *Technical Report* PhD Thesis, GKSS-Forschungszentrum Geesthacht GmbH, GKSS Library, Postfach 11 60, D-21494 Geesthacht, 2008.
20. Troen I, Petersen EL. *European Wind Atlas*. Risø National Laboratory: Roskilde, 1989.
21. Tennekes H. Similarity relations, scaling laws and spectral dynamics. In *Atmospheric Turbulence and Air Pollution Modelling*. Nieuwstadt FTM, van Dop H (eds). D. Reidel Publishing Company: Dordrecht, 1982; 37–68.
22. Landberg L, Myllerup L, Rathmann O, Petersen EL, Jørgensen BH, Badger J, Mortensen NG. Wind resource estimation—an overview. *Wind Energy* 2003; **6**: 261–271.
23. Charnock H. Wind stress on a water surface. *Quarterly Journal of the Royal Meteorological Society* 1955; **81**: 639–640.
24. Frank HP. Extreme winds over Denmark from the NCEP/NCAR reanalysis. *Technical Report Risoe-R-1238(EN)*, Risø National Laboratory, Roskilde, http://www.risoe.dk/rispubl/VEA/ris-r-1238.htm, 2001.
25. Miller C. A once in 50-year wind speed map for Europe derived from mean sea level pressure measurements. *Journal of Wind Engineering and Industrial Aerodynamics* 2003; **91**: 1813–1826.
26. Pryor SC, Nielsen M, Barthelmie RJ, Mann J. Can satellite sampling of offshore wind speeds realistically represent wind speed distributions? Part II: quantifying uncertainties associated with sampling strategy and distribution fitting methods. *Journal of Applied Meteorology* 2004; **43**: 739–750.
27. Hasager CB, Barthelmie R, Christiansen MB, Nielsen M, Pryor SC. Quantifying offshore wind resources from satellite wind maps: study area the North Sea. *Wind Energy* 2006; **9**: 63–74.
28. Barthelmie RJ, Pryor SC. Can satellite sampling of offshore wind speeds realistically represent wind speed distributions? *Journal of Applied Meteorology* 2003; **42**: 83–94.
29. Gielbel G. On the benefits of distributed generation of wind energy in Europe. *Technical Report* PhD Thesis, Nr 444, Carl von Ossietzky Universität Oldenburg, VDI-Verlag, Schriftenreihe Energietechnik, http://www.drgiebel.de/GGiebel_DistributedWindEnergyInEurope.pdf, 2007.
30. Gielbel G. A variance analysis of capacity displaced by wind energy in Europe. *Wind Energy* 2007; **10**: 69–79.
31. Pope SB. *Turbulent Flows*. Cambridge University Press: Cambridge, 2000.
32. Robeson SM, Shein KA. Spatial coherence and decay of wind speed and power in the North-Central United States. *Physical Geography* 1997; **18**: 479–495.
33. Sørensen P, Larsén XG, Mann J, Cutululis NA. Modelling wind turbine cut outs in a power system region. In *Proceedings: Nordic Wind Power Conference (NWPC 2007), 1–2 November 2007*. Cutululis NA, Sørensen P (eds). Risø-R-1624 (EN), Risø: Copenhagen, 2007; 212–215.